J Mater Sci (2016) 51:10990–11001

Phase selection and re-melting-induced anomalous eutectics in undercooled Ni–38 wt% Si alloys

Cun Lai[1], Haifeng Wang[1,*], Qian Pu[1], Tingting Xu[1], Jinsong Yang[1], Xi Zhang[1], and Feng Liu[1,*]

[1] *State Key Laboratory of Solidification Processing, Northwestern Polytechnical University, Xi'an 710072, Shaanxi, People's Republic of China*

Received: 9 May 2016
Accepted: 17 August 2016
Published online: 30 August 2016

ABSTRACT

The Ni–38 wt% Si alloy whose eutectic products are two stoichiometric intermetallic compounds (i.e., NiSi and $NiSi_2$) was undercooled by the melt fluxing technique. After in situ observations of the recalescence processes using a high-speed camera and by electron back-scattering diffraction analysis of the solidification microstructures, the crystal growth velocities, phase selection, and microstructure evolutions were studied. Due to a growth-controlled mechanism, the primary phase changes from the NiSi to the $NiSi_2$ phase at a critical undercooling $\Delta T \approx 48$ K. Even in the absence of the driving force of chemical superheating, the transition from regular eutectics to anomalous eutectics happens. The reason is that the single-phase dendrite of $NiSi_2$ phase solidifies firstly and then the NiSi phase grows epitaxially to form an uncoupled eutectic-dendrite at high undercooling. The present work provides further experimental evidences for the dual origins of anomalous eutectics (e.g., uncoupled eutectic-dendrite growth during the recalescence stage and coupled lamellar eutectic growth at low undercooling during the post-recalescence stage) and is helpful for understanding of non-equilibrium phenomena in undercooled melts.

Introduction

Eutectic alloys are of major practical importance ascribing to their good casting, wetting, and mechanical properties [1]. Due to different solidification conditions, physical properties, and volume fractions of eutectic phases, an extensive variety of eutectic morphologies exhibit [2–7]. Taking the case of undercooling as an example, a well-known non-equilibrium phenomenon is the transition from regular eutectics to anomalous eutectics (e.g., in the Ag–Cu [8, 9], Co–Si [10, 11], Co–Sn [12–14], and Ni–Sn [15–18] alloys), the mechanism of which has been studied extensively [12–21].

In the undercooled Ag–Cu eutectic alloy, two types of eutectic microstructures, i.e., "lamellar" and "anomalous" eutectics, were found by Powell and Hogan [19]. The anomalous eutectics were suggested to be formed by a repeated nucleation of Cu-rich solid-solution phase ahead of the growing matrix of Ag-rich solid-solution phase. In the undercooled Ni–Sn eutectic alloy, Kattamis and Flemings [17] found

Address correspondence to E-mail: haifengw81@nwpu.edu.cn; liufeng@nwpu.edu.cn

DOI 10.1007/s10853-016-0312-y

that the anomalous eutectics were of a "dendrite-like" morphology. After successively polishing and examining the microstructures of parallel sections, both phases in the anomalous eutectics were found to be interconnected along a polyhedral network. Accordingly, they suggested that the initial "dendrite-like" microstructure should be a precipitation of supersaturated single α-Ni solid-solution phase, subsequent decomposition of which during the post-recalescence stage forms the anomalous eutectics with α-Ni and β-Ni_3Sn phases. In contrast, Jones [20] found neither dendritic branching nor continuous network of both phases in the undercooled Ag–Cu eutectic alloy and attributed the formation of anomalous eutectics to uncoupled eutectic growth. Such mechanism was followed by Li et al. [12] who ascribed uncoupled eutectic growth to extremely diverse linear kinetic coefficients of eutectic phases. Wei et al. [21], however, proposed that the two eutectic phases nucleated independently and grew cooperatively, i.e., coupled eutectic-dendrite growth should be responsible for the formation of anomalous eutectics.

According to their experimental results in the undercooled Ni–Si, Co–Sb, and Ni–Al–Ti eutectic alloys, Goetzinger et al. [23] suggested that the fragmentation of primary eutectic lamellae with the reduction of interfacial energy as the driving force leads to the formation of anomalous eutectics. Based on the in situ observations of the recalescence processes in which a double recalescence was found during spasmodic growth, Clopet et al. [9] ascribed the origin of anomalous eutectics in the undercooled Ag–Cu alloy to re-melting of eutectic-dendrites. Li et al. [22] supposed that the anomalous eutectics are formed by both coupled and uncoupled eutectic growth in the undercooled Ni–Sn eutectic alloy. At low undercooling, anomalous eutectics are formed by fragmentation and ripening of lamellar eutectics. At high undercooling, uncoupled eutectic growth (or re-melting of the primary single dendritic phase and subsequent crystallization of the second phase from the inter-dendritic liquid) gives rise to the anomalous eutectics. Such a mechanism of dual origins was proved further by in situ observations and electron back-scattering diffraction (EBSD) analysis of undercooled Ni–Sn eutectic alloy [15].

In the very recent work of Wei et al. [4], the re-melted fraction of primary eutectics was analyzed systematically according to the eutectic-dendrite growth theory and was suggested to be an indicator of the tendency for the formation of anomalous eutectics. After a comparison among three representative binary eutectic alloys (i.e., Ag–39.9 at.% Cu, Ni–19.6 at.% P, and Pd–16.0 at.% P alloys whose eutectic products are solid solution–solid solution, solid solution–stoichiometric intermetallic compound, and stoichiometric intermetallic compound–stoichiometric intermetallic compound, respectively), it was concluded that anomalous eutectics are formed by re-melting of primary solid during solidification of undercooled eutectic alloy melts. The dominative driving force for re-melting should be the chemical superheating regardless of whether the primary solid consists of a single-phase or eutectic microstructure. The reduction of interfacial energy plays a role when superheating-induced re-melting takes place and promotes the fragmentation during the post-recalescence stage. The recent work above [4, 9, 15, 22, 23] shows that re-melting is the primary mechanism for the formation of anomalous eutectics. However, whether the dominative driving force for re-melting is the reduction of interfacial energy because solids attempts to minimize its surface areas via heat and solute diffusions [23] or the chemical superheating [4] because the non-equilibrium supersaturated primary solid evolves to the equilibrium state by excluding redundant solute is still an open problem.

In the present work, rapid solidification of undercooled Ni–38 wt% Si alloy whose eutectic products are two stoichiometric intermetallic compounds (i.e., NiSi and $NiSi_2$) was carried out. The reasons for choosing this alloy system are as follows: (I) The composition of stoichiometric intermetallic does not change with undercooling, thus eliminating the chemical superheating effect and leaving the reduction of interfacial energy as the only driving force for re-melting [4]. (II) According to the Ni–Si phase diagram [24], there are no phase transformations except for the eutectic solidification. Consequently, the primary eutectic microstructure during the recalescence stage and/or re-melting process during the post-recalescence stage could be retained to the room temperature. After in situ observations using a high-speed camera and by EBSD analysis of the solidification microstructures, phase selection between the NiSi and $NiSi_2$ phases was found to be due to a growth-controlled mechanism. The present work shows that the transition from regular eutectics to anomalous eutectics happens even in the absence of

the driving force of chemical superheating and provides further experimental evidences for the dual origins of anomalous eutectics [22], e.g., uncoupled eutectic-dendrite growth during the recalescence stage and coupled lamellar eutectic growth during the post-recalescence stage.

Experimental

A high-purity ingot with a weight of 50 g of Ni–38 wt% Si eutectic alloy was prepared by the pure nickel (99.99 %) and silicon (99.999 %). The master alloy was re-melted for at least three times to ensure chemical homogeneity in the arc furnace facility under a high-purity Ar atmosphere. The final mass loss was found to be within 0.3 %.

The melt fluxing technique was applied to undercool the Ni–38 wt% Si eutectic alloy. A quartz glass crucible, which was rinsed previously in an alcoholic solution by an ultrasonic cleaning machine, was chosen as the container. The sample with a weight of about 2 g was cut from the master alloy and put into the quartz glass crucible with a certain quantity of glass flux of boron oxide. The melt fluxing of boron oxide was used to restrain heterogeneous nucleation within the melts by removing impurities and surface oxides away from the sample and isolating the melts from the surface of the crucible. The quartz glass crucible was located within the high-frequency induction coil of a chamber which was evacuated firstly to a pressure of 3×10^{-3} Pa and then back-filled by a high-purity Ar gas to a pressure of 5×10^{-2} MPa.

The sample was heated firstly to 500 K for about 30 min, which is higher than its melting point of boron oxide but lower than the eutectic temperature of Ni–38 wt% Si alloy 1239 K. Then, the sample covered by the melt fluxing was overheated to 100–250 K above the eutectic temperature and held for about 20 min. Each sample was cyclically superheated and cooled down until a desired undercooling was obtained. The cooling history was recorded by a one-color pyrometer with a response time of 1 ms. The recalescence process was captured using a high-speed camera (OLYMPUSI-Speed 3 MONO). The frame rate was set to be 400–1500 fps according to the duration of recalescence. With the help of software (i-SPEED Software Suite), the average crystal growth velocities were measured by dividing the total traveling distance of the growth front by the solidification time.[1] The as-solidified sample was mounted in Bakelite and carefully polished. After etching in a solution of 10 mL H_2O_2, 10 mL HCl, and 50 mL H_2O, the sample was observed by an optical microscopy (Olympus GX71). The grain orientations were measured using a scanning electron microscope (TESCAN VEGA 3 LMU) with an EBSD analysis system after polishing the sample with the SiO_2 colloidal suspension in a vibratory polisher.

Results

Cooling histories

Figure 1 shows the cooling histories of samples with different undercooling $\Delta T \approx 3$ K, $\Delta T \approx 15$ K, $\Delta T \approx 31$ K, $\Delta T \approx 51$ K, and $\Delta T \approx 74$ K. For $\Delta T \approx 3$ K, the sample solidifies under a near-equilibrium condition and only one thermal plateau that corresponds to eutectic solidification is available. For $\Delta T \approx 15$ K, the superheated melt cools down to 1224 K and then heats up to the eutectic temperature of 1239 K. After a thermal plateau of about 21 s, the temperature decreases monotonously. When the undercooling becomes much larger, e.g., $\Delta T \approx 31$ K, $\Delta T \approx 51$ K and $\Delta T \approx 74$ K, two recalescence events are available in the cooling history. For all the three undercooling, the second recalescence seems to occur within the first recalescence process. Regarding that the onset temperature of second recalescence is higher than that of the first one, the undercooling ΔT in the present work is defined as the difference between the onset temperature of first recalescence and the eutectic temperature. The measured cooling curves (Fig. 1) suggest possibly that two rapid solidification processes that correspond to the two recalescence events happen in relative high undercooled Ni–38 wt% Si eutectic alloys. It should be pointed out that the critical undercooling for the onset of two recalescence events is $\Delta T \approx 20$ K (Fig. 3).

[1] It should be mentioned that in recent work by Binder et al. [25], the high-speed video data with the help of POV-Ray were fitted assuming a reasonable overall shape of the growing phase (e.g., a spherical envelope) to obtain the growth velocity. Such a method should be more reliable than but is not adopted by the current work.

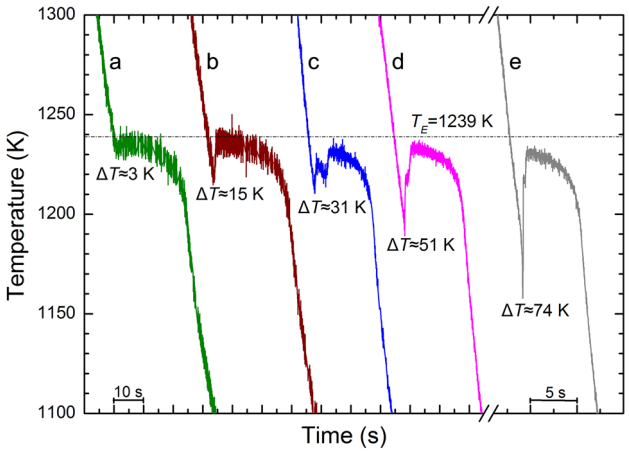

Figure 1 Cooling histories of solidification of Ni–38 wt% Si eutectic alloys with different undercooling: **a** $\Delta T \approx 3$ K, **b** $\Delta T \approx 15$ K, **c** $\Delta T \approx 31$ K, **d** $\Delta T \approx 51$ K, **e** $\Delta T \approx 74$ K.

Recalescence behaviors and crystal growth velocities

Figure 2 shows a typical series of high-speed video camera images of the recalescence processes for $\Delta T \approx 51$ K. The initial (nucleation) points for the first and the second recalescence processes are marked by solid circles. Although the second recalescence seems to occur within the first recalescence process according to the cooling history (Fig. 1), growth of the recalescence front during the first recalescence process has completed before the onset of second recalescence (Fig. 2). For each recalescence process, the recalescence front migrates across the sample surface from one side to the other side, and the solidification microstructures show directional characters at low and high undercooling (see the following section), indicating that it is reasonable to obtain the crystal growth velocity quantitatively by tracking the loci of the recalescence front recorded in the video images at different moments [15]. The determined crystal growth velocities of two recalescence processes are summarized in Fig. 3. For the first recalescence process, an abrupt increase happens at $\Delta T \approx 40$ K, whereas for the second recalescence process, the growth velocity increases monotonously with undercooling and changes from a power law to a linear law [26] at $\Delta T \approx 40$ K. The regions I–V are defined according to the solidification microstructures in which the cases of a-e marked by the open circles are shown in the next section, i.e., Fig. 4.

Microstructures and EBSD analysis

Figure 4 shows the optical micrographs of samples with $\Delta T \approx 3$ K, $\Delta T \approx 15$ K, $\Delta T \approx 31$ K, $\Delta T \approx 51$ K, and $\Delta T \approx 74$ K that correspond to a–e in the regions I–V of Fig. 3, respectively. For $\Delta T \approx 3$ K (or region I), the microstructure is a typical thin regular lamellar eutectics. For $\Delta T \approx 15$ K (or region II), a primary directional granular structure of NiSi phase is surrounded by the thin regular lamellar eutectics. For the region III, e.g., at $\Delta T \approx 31$ K, the primary NiSi phase is surrounded by a coarse eutectic structure, and the

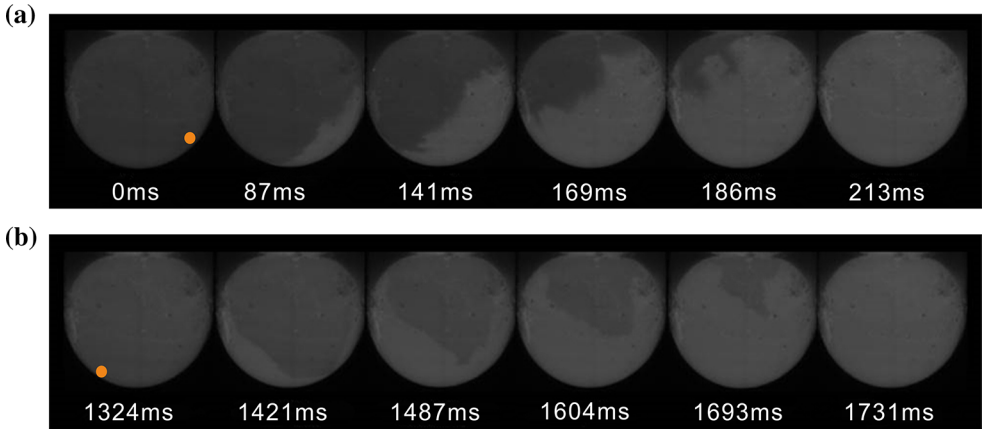

Figure 2 High-speed video camera images showing the recalescence fronts on the surface of Ni–38 wt% Si eutectic alloy with an undercooling of $\Delta T \approx 51$ K: **a** The first recalescence, **b** the second recalescence. The *dark part* and *light part* correspond to the undercooled liquid and recalescing solid, respectively. The initial (nucleation) points for the first and the second recalescence processes are marked by *solid circles*. With the help of software (i-SPEED Software Suite), the average crystal growth velocities for the first and the second recalescence processes are determined as 40.03 and 20.56 mm/s, respectively.

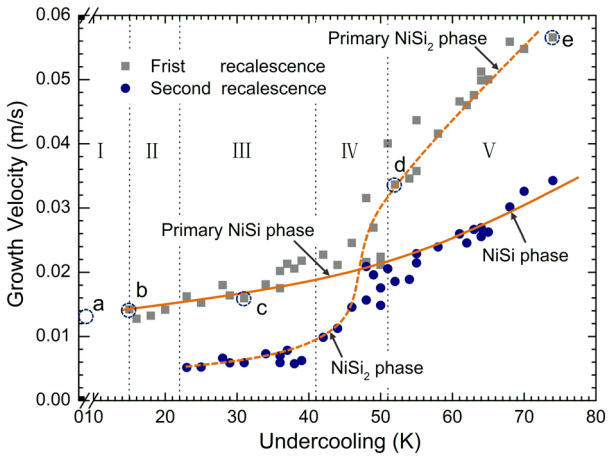

Figure 3 Crystal growth velocity versus undercooling of solidification of Ni–38 wt% Si eutectic alloys. The *solid squares* and *solid circles* correspond to the first and the second recalescence processes, respectively. The regions I–V are defined according to the microstructures in which the cases of *a–e* marked by the open circles are presented in Fig. 4. The *solid line* and the *dotted line* are drew qualitatively for the growth of the NiSi and $NiSi_2$ phases, according to which the critical undercooling for the transition of primary phase from the NiSi to the $NiSi_2$ phase is found to be at the critical undercooling $\Delta T \approx 48$ K.

rest is the thin regular lamellar eutectics. For $\Delta T \approx 51$ K (or region IV), strip-shaped NiSi structures and dendritic $NiSi_2$ phase are found together with the thin regular lamellar eutectics. At the maximal undercooling obtained in the present work $\Delta T \approx 74$ K (or region V), NiSi and $NiSi_2$ eutectic-dendrites are prevailed. In some regions, the eutectic-dendrites are fragmented into anomalous eutectics. It should be pointed out that all the microstructures consist solely of the NiSi and $NiSi_2$ phases according to the XRD and EDS results. In order to show the mechanism of microstructure evolutions, EBSD analysis was carried out, and the results are shown as follows.

The EBSD orientation maps and the {100} pole figures (PFs) of the Ni–38 wt% Si eutectic alloy solidified at $\Delta T \approx 3$ K are shown in Fig. 5a–d. The NiSi (Fig. 5a) and $NiSi_2$ (Fig. 5c) phases have almost one single color. From the PFs, only one main orientation can be found for the NiSi (Fig. 5b) and the $NiSi_2$ (Fig. 5d) phase, being consistent with cooperative growth of lamellar eutectics. Figure 6 shows the EBSD orientation maps and the {100} PFs for the case of $\Delta T \approx 15$ K. Three main orientations are found for the NiSi phase, even though the differences between the orientations are not that large. Because the granular structure and the surrounding regular lamellar of NiSi phases share the same orientation, the lamellar eutectics should be formed by an epitaxial growth mechanism. Correspondingly, the regular lamellar of $NiSi_2$ also has three main orientations.

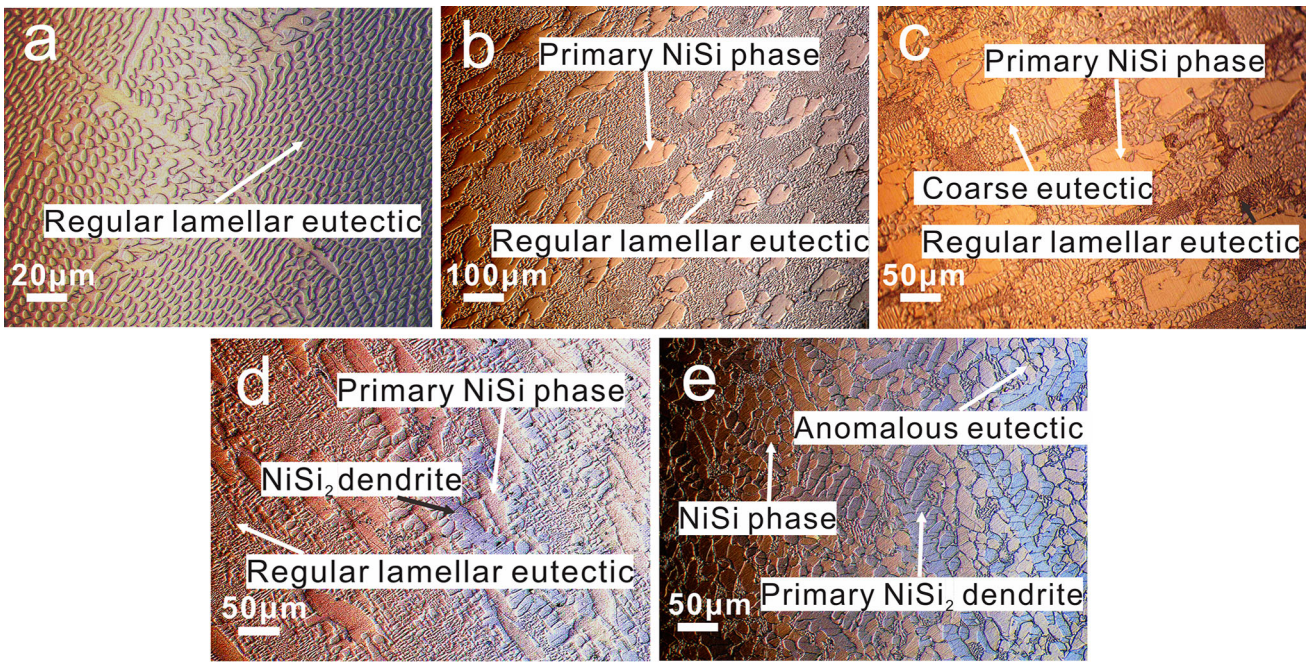

Figure 4 Typical optical micrographs corresponding to the regions I–V defined in Fig. 3: **a** $\Delta T \approx 3$ K, **b** $\Delta T \approx 15$ K, **c** $\Delta T \approx 31$ K, **d** $\Delta T \approx 51$ K, **e** $\Delta T \approx 74$ K.

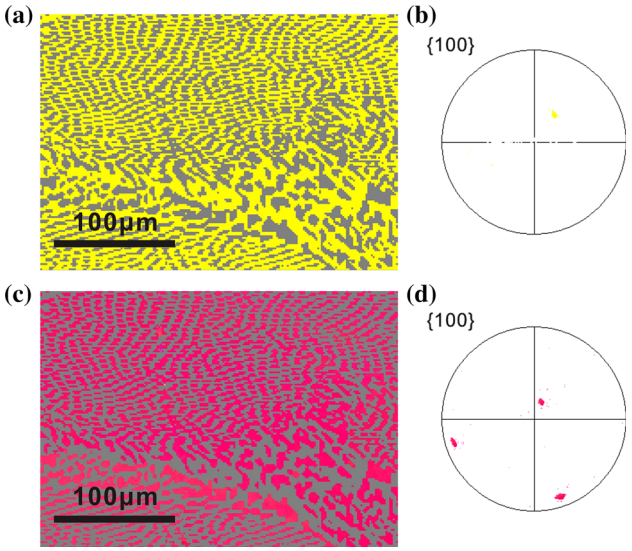

Figure 5 EBSD analysis of regular lamellar eutectic microstructure of the Ni–38 wt% Si eutectic alloy with an undercooling of $\Delta T \approx 3$ K. **a** EBSD orientation map and **b** {100} pole figure of NiSi phase. **c** EBSD orientation map and **d** {100} pole figure of $NiSi_2$ phase.

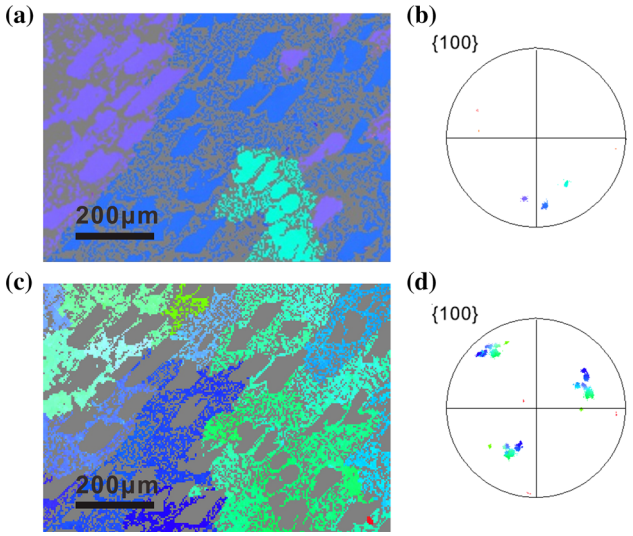

Figure 6 EBSD analysis of primary granular NiSi structure and regular lamellar eutectic microstructure of the Ni–38 wt% Si eutectic alloy with an undercooling of $\Delta T \approx 15$ K. **a** EBSD orientation map and **b** {100} pole figure of NiSi phase. **c** EBSD orientation map and **d** {100} pole figure of $NiSi_2$ phase.

Although only one recalescence event can be found in the cooling history (Fig. 1), two transformation processes can be distinguished from the solidification microstructures, i.e., the primary crystal growth of NiSi phase and the second lamellar eutectic growth of NiSi and $NiSi_2$ phases.[2] Furthermore, the granular structure of NiSi might be formed by an initial strip-shaped structure which is fragmented during the post-recalescence stage.

Figure 7 shows the EBSD orientation maps and the {100} PFs for the case of $\Delta T \approx 31$ K. For the NiSi phase, only one main orientation is available, indicating that both the coarse eutectic structure and the thin regular lamellar eutectics are formed by an epitaxial growth mechanism. For the $NiSi_2$ phase, however, three main orientations are found, the orientation differences between which are rather large. Furthermore, the green grain shares one

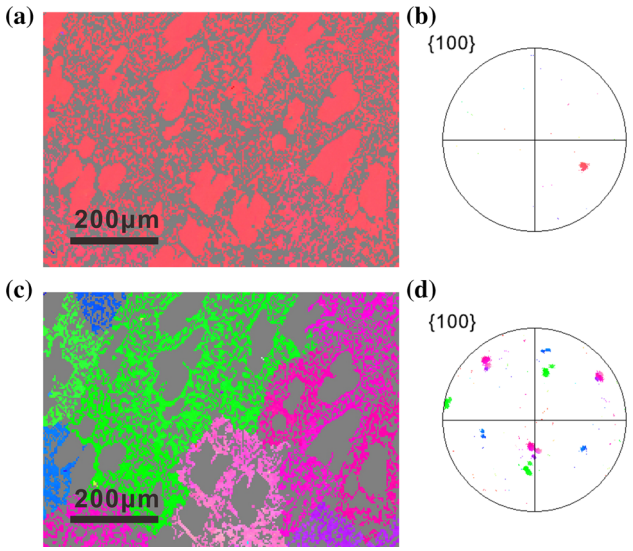

Figure 7 EBSD analysis of primary granular NiSi structure surrounding successively by a coarse eutectic structure and a thin lamellar eutectic of the Ni–38 wt% Si eutectic alloy with an undercooling of $\Delta T \approx 31$ K. **a** EBSD orientation map and **b** {100} pole figure of NiSi phase. **c** EBSD orientation map and **d** {100} pole figure of $NiSi_2$ phase.

concentrated pole with the blue and the pink grain in the PF (Fig. 7d), indicating the orientation relationships for cooperative growth could be diversified. An explanation of such phenomenon is however out of

[2] This is similar to the work by Li et al [27], in which the Co–61.8 at.% Si eutectic alloy was undercooled by both an electromagnetic levitator and an electrostatic levitator. At low undercooling, only a single recalescence event can be found but the microstructure consists of primary CoSi phase and CoSi–$CoSi_2$ eutectics. In subsequent work by Zhang et al. [11], the recalescence behaviors of undercooled Co–61.8 at.% Si eutectic alloy are much more complex; please see their Fig. 1. All these results indicate that the transformation process and the recalescence behaviors may not follow the one-to-one relationship.

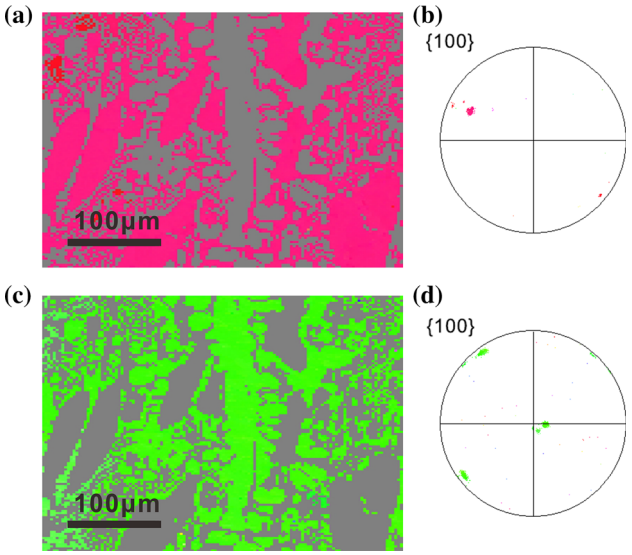

Figure 8 EBSD analysis of primary strip-shaped NiSi structures and $NiSi_2$ dendrite of the Ni–38 wt% Si eutectic alloy with an undercooling of $\Delta T \approx 51$ K. **a** EBSD orientation map and **b** {100} pole figure of NiSi phase. **c** EBSD orientation map and **d** {100} pole figure of $NiSi_2$ phase.

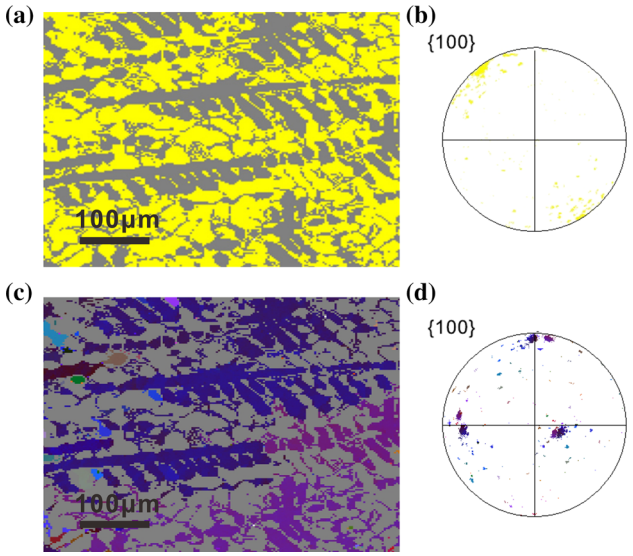

Figure 9 EBSD analysis of the region of eutectic-dendrite (NiSi and $NiSi_2$) of the Ni–38 wt% Si eutectic alloy with an undercooling of $\Delta T \approx 74$ K. **a** EBSD orientation map and **b** {100} pole figure of NiSi phase. **c** EBSD orientation map and **d** {100} pole figure of $NiSi_2$ phase.

the scope of the present work. In the case of $\Delta T \approx 31$ K, two recalescence events are found in the cooling history (Fig. 1a). It is quite reasonable to speculate that the first (second) recalescence corresponds to the formation of primary granular structure of NiSi phase and subsequent growth of NiSi phase in the coarse eutectic structure (epitaxial growth of $NiSi_2$ phase in the coarse eutectic structure). The thin lamellar eutectic is solidified during the post-recalescence stage.[3]

Figure 8 shows the EBSD orientation maps and the {100} PFs for the case of $\Delta T \approx 51$ K. For both the NiSi and the $NiSi_2$ phases, only one main orientation can be found. In this case, the coarse strip-shaped NiSi structure and the $NiSi_2$ dendrite coexist, both of which could be the primary phase that is crystalized during the first recalescence stage. Integrating with the experimental results of $\Delta T \approx 74$ K (Figs. 9, 10), however, the $NiSi_2$ dendrite should be the primary phase that forms in the first recalescence stage and

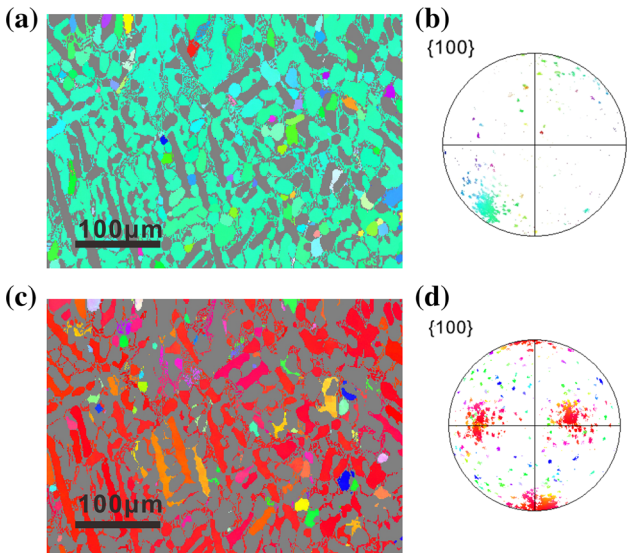

Figure 10 EBSD analysis of the region of fragmentation of eutectic-dendrite (NiSi and $NiSi_2$) of the Ni–38 wt% Si eutectic alloy with an undercooling of $\Delta T \approx 74$ K. **a** EBSD orientation map and **b** {100} pole figure of NiSi phase. **c** EBSD orientation map and **d** {100} pole figure of $NiSi_2$ phase.

then the coarse strip-shaped NiSi structure is crystallized epitaxially during the second recalescence stage. The remained liquid solidifies finally as the thin regular lamellar eutectics during the post-recalescence stage.

[3] It should be noted that for coupled growth, the lamellar spacing of eutectic formed at high undercooling should be smaller than that formed at low undercooling. The present coarse eutectic is formed by uncoupled growth but not coupled growth. Therefore, it is not strange that the lamellar spacing of the present coarse eutectic formed at high undercooling is larger than that of the thin lamellar eutectic formed at low undercooling.

For the case of $\Delta T \approx 74$ K, the EBSD orientation maps and the {100} PFs are shown in Figs. 9 and 10. Besides some random orientations, only one main orientation can be found for both the NiSi and the $NiSi_2$ phases. For the eutectic-dendrite region, the $NiSi_2$ phase is of a well-developed dendritic microstructure, while the NiSi phase grows epitaxially to form a eutectic-dendrite. This kind of eutectic-dendrite grows by not a coupled but an uncoupled mechanism in which the primary $NiSi_2$ dendrite is formed during the first recalescence stage, and the NiSi phase is solidified during the second recalescence stage.[4] In the inter-eutectic-dendrite region, fine eutectic structures can be observed. For the region with fragmentation, the characters of orientations are similar except that the random orientations become more. For the $NiSi_2$ phase, the dendrites are re-melting into strip-shaped and coarse granular structures. For the NiSi phase, fragmentation is also prevailed. For the $NiSi_2$ and NiSi phases with the interfacial energy as the only driving force for re-melting, the re-melting process cannot take place so adequately that the fragmentation does not have the time and the chance to be moved far away from their origins and rotated with large angles (Figs. 9a, c, 10a, c). Consequently, the intermediate fragmentation process can be retained to show the mechanism and the origin of anomalous eutectics.

Discussion

Mechanism of phase selection

In the undercooled Ni–38 wt% Si eutectic alloy, the primary phase changes from the NiSi to the $NiSi_2$ phase with the increase of undercooling, i.e., phase selection occurs. In a similar Co–61.8 at.% Si eutectic alloy in which CoSi is a non-stoichiometric intermetallic compound and $CoSi_2$ is a stoichiometric intermetallic compound, a transition from the CoSi to the $CoSi_2$ phase occurs [10, 11, 25]. Li et al. [25] expected that the two intermetallic compounds have a similar short-range diffusion-controlled growth mechanism at the solid/liquid interface because the CoSi and $CoSi_2$ phases share the same simple cubic lattice structure. Since the melting temperature of CoSi phase (1460 °C) is much larger than that of $CoSi_2$ phase (1326 °C) and the interface energies are roughly proportional to the melting temperature, the interfacial energy of CoSi phase should be higher than that of $CoSi_2$ phase. Regarding that the critical nucleation barrier is proportional to the cube of the interfacial energy, nucleation of $CoSi_2$ phase is preferred at high undercooling. Yao et al. [10] found that the $CoSi_2$ phase has a lower nucleation rate than that of the CoSi phase but grows faster over a wide range of undercooling. Recently, Zhang et al. [11] calculated the critical work of nucleation and found that the $CoSi_2$ phase has lower critical work of nucleation when the undercooling is larger than the critical undercooling where the transition of primary phase happens. All the previous work [10, 11, 25] shows that phase selection in undercooled Co–61.8 at.% Si eutectic alloys are nucleation controlled.

Actually, phase selection is quite a common non-equilibrium phenomenon in undercooled melts and the mechanisms can be classified into two categories, i.e., nucleation controlled and growth controlled [27, 29, 30]. In the present work, the NiSi phase is of an orthogonality primitive lattice structure (*oP*8) with a space group *Pnma*, and the $NiSi_2$ pase is of a face-centered cubic lattice structure (*cF*12) with a space group *Fm3 m*. According to the Ni–Si phase diagram [24], the melting temperature of the NiSi phase is 1265 K, but the melting temperature of the $NiSi_2$ phase cannot be obtained directly because of the peritectic transformation $L + \mathrm{Si} \rightarrow \mathrm{NiSi_2}$. According to the thermodynamic assessment of the Ni–Si system [31], the melting temperatures of the NiSi and $NiSi_2$ phases are calculated to be 1258 and 1282 K, respectively. If the lattice structure difference between the NiSi and $NiSi_2$ phase is omitted and the viewpoint of Li et al. [27] is followed, the difference between the melting temperatures 24 K is so small that the nucleation-controlled mechanism should not play a dominative role in phase selection.

In the present work, the crystal growth velocities are measured for both the first and the second recalescence processes (Fig. 3). At low undercooling, the primary phase is the NiSi phase, and the growth

[4] Eutectic-dendrite can be defined as a dendrite on the whole, the solids of which are formed by eutectic solidification. There are two kinds of eutectic-dendrite according to the growth mechanism, i.e., by coupled and uncoupled eutectic growth. For the former, other alloy element should be added to the eutectic alloy or a negative temperature gradient should be improved to the eutectic interface to make the interface unstable to a dendritic morphology. This is the physical basis for the current eutectic-dendrite growth theory [2, 23, 28]. For the latter, the primary dendrite phase is followed by solidification of a second phase.

velocity of the first recalescence is larger than that of the second recalescence. Taking the case of $\Delta T \approx 31$ K as an example, the NiSi and $NiSi_2$ phases are crystallized in the first and the second recalescence processes, respectively. The growth velocity of NiSi phase is larger than that of the $NiSi_2$ phase. At high undercooling, the primary phase is the $NiSi_2$ phase, and the growth velocity of the first recalescence is larger than that of the second recalescence. Taking the case of $\Delta T \approx 74$ K as an example, the $NiSi_2$ and NiSi phases are crystallized in the first and the second recalescence processes, respectively. The growth velocity of $NiSi_2$ phase is larger than that of NiSi phase. At the intermediate undercooling, the increase of growth velocity in the second recalescence is much faster than that in the first recalescence, and the growth velocities of the first and the second recalescence processes could coincide nearly with each other (Fig. 3). In other words, phase selection between the NiSi and the $NiSi_2$ phase is growth controlled. In order to show the growth-controlled mechanism more clearly, a solid line and a dotted line are drawn qualitatively for the growth of the NiSi and $NiSi_2$ phases in Fig. 3, and the critical undercooling for the transition of primary phase is found to be at $\Delta T \approx 48$ K. For phase selection and metastable phase formation in undercooled Ni–Si alloys with different eutectic compositions, special attention should be paid to the work by Mullis et al. [32–35].

Driving force for re-melting

As already mentioned in the introduction, re-melting has been regarded to be the primary mechanism for the formation of anomalous eutectics. For the driving force of re-melting, Goetzinger et al. [23] proposed that it is the reduction of interfacial energy. Such viewpoint is an extension of the grain refinement theory of dendrite of single solid-solution phase in which a mushy zone exists during the post-recalescence stage [36–38]. In other words, minimization of surface areas happens by heat and solute diffusions in liquid. For regular lamellar eutectic where there is no mushy zone, re-melting cannot happen. In this case, coarsening happens [39], but this process should be quite slow because minimization of surface areas happens by solute diffusion in solid. For undercooled melts, the negative thermal gradient ahead of the eutectic front can make the interface unstable to eutectic cells or eutectic-dendrite [8]. In this case, the mushy zone forms and thus re-melting happens. For uncoupled eutectic-dendrite growth at high undercooling (e.g., Figs. 9, 10), re-melting of the primary phase is similar to that of single-phase dendrite [36–38]. Solidification (and re-melting) of the second phase then forms the coarse anomalous eutectics.

In contrast, Wei et al. [4] proposed that the chemical superheating should be the dominative driving force and the reduction of interfacial energy should be the secondary one. In the case of Pd–16.0 at.% P alloy whose eutectic products are two stoichiometric intermetallic compounds, there is no chemical superheating and thus no anomalous eutectics. For the present Ni–38 wt% Si eutectic alloy whose products are also two stoichiometric intermetallic compounds, anomalous eutectics are formed even in the absence of chemical superheating. Such contradictory results are actually understandable. For the Pd–16.0 at.% P alloy, lamellar eutectic growth happens at high undercooling; please see Fig. 11 in Ref. [4]. There is therefore no mushy zone during the post-recalescence stage and no re-melting by reduction of interfacial energy. For the present Ni–38 wt% Si eutectic alloy, single-phase dendrite of $NiSi_2$ phase is solidified firstly and then the NiSi phase grows epitaxially to form an uncoupled eutectic-dendrite at high undercooling (Fig. 9). In this case, re-melting happens with the reduction of interfacial energy as the only driving force (Fig. 10). Combining the present work with those by Wei et al. [4] and Goetzinger et al. [23], one can see that the dominative driving force for re-melting could be either the chemical superheating, or the reduction of interfacial energy, or both. For both the cases of coupled growth with mushy zone (e.g., coupled eutectic-dendrite) and uncoupled growth (e.g., primary single-phase dendrite or uncoupled eutectic-dendrite), one cannot distinguish absolutely which driving force is the dominative one if both driving forces are present. It should be pointed out that Wei et al. [4] themselves also did not exclude re-melting of primary single-phase dendrite (please see Fig. 5 in Ref. [4]), even though their work is based on the theory of coupled eutectic-dendrite growth.

One can see that there are three kinds of anomalous eutectic, i.e., chemical superheating-induced, reduction of interfacial energy-induced, and chemical superheating-induced and reduction of interfacial

energy-induced anomalous eutectics according to the driving forces. Form origins, there are two kinds of anomalous eutectic: uncoupled eutectic-dendrite growth-formed and coupled lamellar eutectic growth-formed anomalous eutectics. For uncoupled eutectic-dendrite growth, the driving force is the reduction of interfacial energy and the chemical superheating or only the reduction of interfacial energy if the supersaturated primary solid cannot form during rapid solidification. For coupled lamellar eutectic growth without the mushy zone, the chemical superheating is the only driving force. In the present work, lamellar/granular eutectic is available in the inter-eutectic-dendrite region (Figs. 9a, c and 10a, c), re-melting of which could also form the second kind of anomalous eutectic from origins, if there is the driving force of chemical superheating. Therefore, the dual origins of anomalous eutectics [22] are also supported by the present work.

Conclusions

Rapid solidification of undercooled Ni–38 wt% Si alloy whose eutectic products are two stoichiometric intermetallic compounds was observed in situ using a high-speed camera. The crystal growth velocities were measured, and the as-solidified microstructures were analyzed by EBSD. Our main conclusions are as follows:

1. When $\Delta T < 20$ K, there is only one recalescence event, whereas when $\Delta T > 20$ K, there are two recalescence events. For the former, the recalescence corresponds to either eutectic solidification or solidification of primary NiSi phase. For the latter, the first and second recalescence processes correspond with crystallization of NiSi and $NiSi_2$ phase at low undercooling ($NiSi_2$ and NiSi phases at high undercooling), respectively. Phase selection between the NiSi and the $NiSi_2$ phases is growth controlled, and the critical undercooling for the transition is $\Delta T \approx 48$ K.
2. With the increase of undercooling, the microstructure changes in sequence from thin lamellar eutectics, primary granular structure of NiSi phase surrounded by thin regular lamellar eutectics, primary NiSi phase surrounded successively by coarse eutectics and thin regular lamellar eutectics, dendritic $NiSi_2$ phase surrounded by strip-shaped NiSi phase, and thin regular lamellar eutectics to uncoupled eutectic-dendrites and anomalous eutectics.
3. EBSD analysis shows that the NiSi and the $NiSi_2$ phases share only one or some main orientations and the random orientations are limited even when anomalous eutectics form at high undercooling, indicating that the primary eutectic microstructure during the recalescence stage and/or re-melting process during the post-recalescence stage can be retained to the room temperature.
4. The transition from regular eutectics to anomalous eutectics happens even in the absence of the driving force of chemical superheating because the single-phase dendrite of $NiSi_2$ phase is solidified firstly and then the NiSi phase grows epitaxially to from an uncoupled eutectic-dendrite at high undercooling. The dual origins of anomalous eutectics [22], e.g., uncoupled eutectic-dendrite growth during the recalescence stage and coupled lamellar eutectic growth at low undercooling during the post-recalescence stage, are supported by the present experimental results.

Acknowledgements

The authors would like to thank the Natural Science Foundation of China (Nos. 51371149, 51134011 and 51431008), the China National Funds for Distinguished Young Scientists (No. 51125002), Huo Yingdong Young Teacher Fund (No. 151048), the Aeronautical Science Foundation of China (No. 2015ZF53066), the Free Research Fund of State Key Lab. of Solidification Processing (No. 92-QZ-2014) and the project of Shaanxi Young Stars of Science and Technology (No. 2015KJXX-10).

References

[1] Kurz W, Fisher DJ (1979) Dendrite growth in eutectic alloys: the coupled zone. Int Mater Rev 24:177–204

[2] Li JF, Zhou YH (2005) Eutectic growth in bulk undercooled melts. Acta Mater 53:2351–2359

[3] Li JF, Li XL, Liu L et al (2008) Mechanism of anomalous eutectic formation in the solidification of undercooled Ni–Sn eutectic alloy. J Mater Res 23:2139–2148

[4] Wei XX, Lin X, Xu W et al (2015) Remelting-induced anomalous eutectic formation during solidification of deeply undercooled eutectic alloy melts. Acta Mater 95:44–56
[5] Herlach DM (1994) Non-equilibrium solidification of undercooled metallic melts. Mater Sci Eng Rep R 12:177–272
[6] Liu JM, Zhou YH, Shang BL (1992) Theory and experiments on irregular eutectic growth: investigation on Al–Si eutectic growth. J Mater Sci 27:2067–2074
[7] Wang JT, Kang SB, Kim HW et al (2002) Lamellae deformation and structural evolution in an Al–33 % Cu eutectic alloy during equal-channel angular pressing. J Mater Sci 37:5223–5227
[8] Zhao S, Li JF, Liu L et al (2009) Eutectic growth from cellular to dendritic form in the undercooled Ag–Cu eutectic alloy melt. J Cryst Growth 311:1387–1391
[9] Clopet CR, Cochrane RF, Mullis AM (2013) The origin of anomalous eutectic structures in undercooled Ag–Cu alloy. Acta Mater 61:6894–6902
[10] Yao WJ, Wang N, Wei B (2003) Containerless rapid solidification of highly undercooled Co–Si eutectic alloys. Mater Sci Eng A 344:10–19
[11] Zhang YK, Gao J, Kolbe M et al (2013) Phase selection and microstructure formation in undercooled Co–61.8 at.% Si melts under various containerless processing conditions. Acta Mater 61:4861–4873
[12] Li M, Kuribayashi K (2003) Nucleation-controlled microstructures and anomalous eutectic formation in undercooled Co–Sn and Ni–Si eutectic melts. Metall Mater Trans A 34:2999–3008
[13] Liu L, Wei XX, Huang QS et al (2012) Anomalous eutectic formation in the solidification of undercooled Co–Sn alloys. J Cryst Growth 358:20–28
[14] Liu L, Li JF, Zhou YH (2011) Solidification interface morphology pattern in the undercooled Co–24.0 at.%Sn eutectic melt. Acta Mater 59:5558–5567
[15] Yang C, Gao J, Zhang YK et al (2011) New evidence for the dual origin of anomalous eutectic structures in undercooled Ni–Sn alloys: in situ observations and EBSD characterization. Acta Mater 59:3915–3926
[16] Xing LQ, Zhao DQ, Chen XC (1993) Solidification of undercooled Ni–32.5 wt%Sn eutectic alloy. J Mater Sci 28:2733–2737
[17] Kattamis TZ, Flemings MC (1970) Structure of undercooled Ni–Sn eutectic. Metall Trans 1:1449–1451
[18] Cao YQ, Lin X, Wang ZT et al (2015) Three-dimensional reconstruction of anomalous eutectic in laser remelted Ni–30 wt%Sn alloy. Sci Technol Adv Mater 16:1–11
[19] Powell GL, Hogan LM (1965) Undercooling in silver-copper eutectic alloys. J Inst Metals 93:505–512
[20] Jones BL (1971) Growth mechanisms in undercooled eutectic. Metall Trans 2:2950–2951
[21] Wei BB, Yang GC, Zhou YH (1991) High undercooling and rapid solidification of Ni–32.5%Sn eutectic alloy. Acta Metall Mater 39:1249–1258
[22] Li JF, Jie WQ, Zhao S et al (2007) Structural evidence for the transition from coupled to decoupled growth in the solidification of undercooled Ni–Sn eutectic melt. Metall Mater Trans A 38:1806–1816
[23] Goetzinger R, Barth M, Herlach DM (1998) Mechanism of formation of the anomalous eutectic structure in rapidly solidified Ni–Si, Co–Sb and Ni–Al–Ti alloys. Acta Mater 46:1647–1655
[24] Nash P, Nash A (1987) The Ni–Si (Nickel–Silicon) system. Bull Alloy Phase Diagr 8:6–14
[25] Binder S, Galenko PK, Herlach DM (2014) The effect of fluid flow on the solidification of Ni_2B from the undercooled melt. J Appl Phys 115:053511
[26] Wang HF, Liu F, Chen Z et al (2007) Effect of non-linear liquidus and solidus in undercooled dendrite growth: a comparative study in Ni–0.7 at.%B and Ni–1 at.%Zr systems. Scr Mater 57:413–416
[27] Li MJ, Nagashio K, Ishikawa T et al (2008) Microstructure formation and in situ phase identification from undercooled Co–61.8 at.%Si melts solidified on an electromagnetic levitator and an electrostatic levitator. Acta Mater 56:2514–2525
[28] Kuang WW, Wang HF, Liu F et al (2016) Modeling of eutectic dendrite growth in undercooled binary alloys. J Mater Sci 51:2141–2152
[29] Boettinger WJ, Coriell SR, Greer AL et al (2000) Solidification microstructures: recent developments, future directions. Acta Mater 48:43–70
[30] Wei XX, Xu W, Kang JL et al (2016) Metastable $Co_{23}B_6$ phase solidified from deeply undercooled $Co_{79.3}B_{20.7}$ alloy melt. J Mater Sci 51:6436–6443
[31] Tatsuya T, Kazumasa N, Hiroshi O et al (2003) Thermodynamic assessment of the Ni–Si system by incorporating ab initio energetic calculations into the CALPHAD approach. CALPHAD Comput Coupling Phase Diagr Thermochem 27:161–168
[32] Ahmad R, Cochrane RF, Mullis AM (2012) The formation of regular αNi-γ($Ni_{31}Si_{12}$) eutectic structures from undercooled Ni–25 at.%Si melts. Intermetallics 22:55–61
[33] Cao LG, Cochrane RF, Mullis AM (2014) Lamella structure formation in drop-tube processed Ni–25.3 at.%Si alloy. J Alloys Compd 615:S599–S601
[34] Dutra AT, Milenkovic S, Kiminami CS et al (2004) Microstructure and metastable phase formation in a rapidly solidified Ni–Si eutectic alloy using a melt-spinning technique. J Alloys Compd 381:72–76

[35] Cao LG, Cochrane RF, Mullis AM (2015) Microstructural evolution and phase formation in rapidly solidified Ni–25.3 at.%Si alloy. Metall Mater Trans A 46:4705–4715

[36] Schwarz M, Karma A, Eckler K et al (1994) Physical mechanism of grain refinement in solidification of undercooled melts. Phys Rev Lett 73:1380–1383

[37] Karma A (1998) Model of grain refinement in solidification of undercooled melts. Int J Non-Equilib Process 11:201–233

[38] Wang HF, Liu F, Tan YM (2011) Modeling grain refinement for undercooled single-phase solid-solution alloys. Acta Mater 59:4787–4797

[39] Cline HE (1971) Shape instabilities of eutectic composites at elevated temperatures. Acta Metall 19:481–490